Program Digest, 2019 IEEE International Ultrasonics Symposium (IUS)
Glasgow, Scotland, October 6-9, 2019

Total Focusing Method with Subsampling in Space and Frequency Domain for Ultrasound NDT

Eduardo Pérez[1], Jan Kirchhof[1,2], Sebastian Semper[1], Fabian Krieg[1,2], Florian Römer[2]
[1]Technische Universität Ilmenau, Ilmenau, Germany,
[2]Fraunhofer Institute for Nondestructive Testing IZFP, Saarbrücken, Germany

***Abstract* — In this paper, we present a compressed sensing model for 2D Full Matrix Capture data from a uniform linear array. Data is reconstructed via a matrix-free implementation of the Total Focusing Method (TFM) combined with the Fast Iterative Shrinkage/ Thresholding Algorithm. This results in reduced measurement times and data volumes without sacrificing image quality. Our approach is compared to standard TFM by applying the techniques on real measurement data, both synthetically compressed and complete.**

I. Introduction and State of the Art

Sampling phased arrays allow the acquisition of so-called *Full Matrix Capture* (FMC) data, enabling the usage of sophisticated post-processing techniques for ultrasound nondestructive testing (UNDT) [1], [2]. One such technique is the *Total Focusing Method* (TFM) [3], a multi-channel extension to the *Synthetic Aperture Focusing Technique* (SAFT) [4]. TFM is attractive due to its high resolution; however it displays limited performance when it comes to distinguishing closely spaced defects. This has roused interest in modifications to TFM that allow it to overcome this shortcoming.

Enhancements to TFM based on forward models are a topic of widespread interest. In [5], the authors cast TFM as a sparse signal recovery task by expressing it as an ℓ_1 regularized inverse problem. Similarly to the approach in [6], the inverse problem formulation is extended in [7] by considering a pulse shape dictionary, further increasing resolution. Anisotropic propagation and frequency-dependent attenuation are included in the forward model in [8] along with an alternative MAP reconstruction approach.

TFM and its variants suffer from the costly FMC process in spite of the achievable resolution. The data capture process requires a separate measurement cycle for each transmitting element in the array. This is time consuming and yields large data volumes. These shortcomings can be overcome through compressed sensing directly during the measurement procedure. In [9], the measurement time is reduced by allowing overlap of different randomly delayed transmit events in the received signals. In this paper, we present a compressed sensing formulation for TFM as an inverse problem to reduce the size of the data set and the measurement time. This is done by first adapting the single-channel Fourier subsampling technique in [10] to the multi-channel case and then extending it with spatial subsampling. The reconstructions obtained through this approach are then compared to those of standard TFM by applying both techniques to measurement data.

Eduardo Pérez and Fabian Krieg are funded by DFG under the project "CoSMaDU". Sebastian Semper is funded by DFG under the project "HoPaDyn". This work was supported by the Fraunhofer Internal Programs under Grant No. Attract 025-601128.

II. FMC Model

In SAFT-like algorithms [3], [4], measurement data is modeled as a weighted sum of pulse echoes whose time delays depend on the geometric relationship between sensors and impedance discontinuities inside a specimen. In the FMC procedure, one transmitter (Tx) transmits a pulse at a time while all receivers (Rx) listen to the echoes, and this is done for all elements in the sensor array. The 2D single measurement channel case of such a model can be expressed as

$$b_{i,j}^{(a)}(t) = \left(\sum_{s=1}^{S} a_s \cdot g_{i,j}(x_s, z_s) \cdot \exp(j\phi_s) \right. \\ \left. \cdot \delta(t - \tau_{i,j}(x_s, z_s)) \right) * h^{(a)}(t), \tag{1}$$

where S is the model order, i.e. number of reflectors, and each reflector has an associated location x_s, z_s and produces an echo with amplitude a_s and phase ϕ_s. Here, the superscript (a) denotes the Hilbert transform. The subindices i, j indicate the Rx and Tx elements that captured the measurement, and $h(\cdot)$ is the pulse shape produced by the Tx element. The positions of the sensors

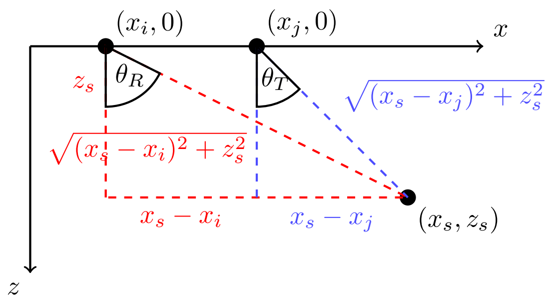

Fig. 1: Illustration of time delay, AOA, and AOD in FMC measurements. These quantities depend on geometric relationships between reflector and sensors.

and flaws result in time delays given by

$$\tau_{i,j}(x_s, z_s) = \frac{\sqrt{(x_s - x_i)^2 + z_s^2} + \sqrt{(x_s - x_j)^2 + z_s^2}}{c_0}.$$

Using the axes shown in Fig. 1, x_i, x_j are the horizontal positions of the Rx, Tx elements, and their common vertical position is set to $z = 0$. If the specimen is homogeneous and isotropic, the speed of sound c_0 is a constant. The term $g_{i,j}(x_s, z_s)$ is an apodization function that accounts for the sensor opening angle θ. We consider a Gaussian apodization function defined as

$$g_{i,j}(x_s, z_s) = \exp\left(\frac{-((x_s - x_i)^2 + (x_s - x_j)^2)}{(\tan(\theta) \cdot z_s)^2}\right).$$

These relationships are illustrated in Fig. 1 along with angles of departure (AOD) and arrival (AOA).

The usage of sampling phased arrays [1], [2] allows the collection of FMC data that can be post-processed with TFM, among other techniques. This data is composed of multiple single-channel measurements of the form (1) sampled at a rate f_s, yielding measurements $\boldsymbol{b}_{i,j}^{(a)} \in \mathbb{C}^{N_T}$. For a uniform linear array (ULA) with M elements, the resulting M^2 single-channel measurements are gathered in $\boldsymbol{b} \in \mathbb{C}^{N_T \cdot M^2}$ such that

$$\boldsymbol{b} = [\boldsymbol{b}_{(j-1)\cdot M + (i-1) + 1}] = [\boldsymbol{b}_{i,j}^{(a)}]_{1 \leqslant i,j \leqslant M}.$$

Next, a 2D array $\boldsymbol{X} \in \mathbb{C}^{N_T \times N_x}$ with elements $x_{k,\ell}$ is used to represent the possible locations of point-like reflectors as a regular grid with resolution Δ_x, Δ_z, where a non-zero entry at element $X_{i,j}$ means that there is a reflector at the corresponding grid point. For simplicity, it is assumed that Δ_z is chosen in relation to f_s so that there are N_T positions along the z direction and the positions in the spatial grid match those in the temporal grid.

The relation between $\boldsymbol{X}$ and $\boldsymbol{b}$ is defined by the linearity assumption and our measurement approach. To clarify this, we describe each vector $\boldsymbol{b}_{i,j}^{(a)}$ as

$$\boldsymbol{b}_{i,j}^{(a)} = \boldsymbol{H} \cdot \boldsymbol{M}_{i,j} \cdot \mathrm{vec}(\boldsymbol{X}), \tag{2}$$

where

$$[\boldsymbol{M}_{i,j}]_{n,m} = g_{i,j}(x_{k,\ell}) \cdot \delta\left(n - \lfloor f_s \cdot \tau_{i,j}(x_{k,\ell}) \rfloor\right), \tag{3}$$

with $m = k \cdot N_x + \ell$ and $\boldsymbol{H}$ being a Toeplitz matrix containing sampled copies of the pulse $h^{(a)}(t)$, and where $\lfloor \cdot \rfloor$ is the floor function. Finally, we arrive at the model

$$\boldsymbol{b} = (\boldsymbol{I}_M \otimes \boldsymbol{I}_M \otimes \boldsymbol{H}) \cdot \boldsymbol{M} \cdot \mathrm{vec}(\boldsymbol{X}), \tag{4}$$

if we define $\boldsymbol{M}$ analogously to $\boldsymbol{b}$. From now on, we will set $\mathrm{vec}(\boldsymbol{X}) = \boldsymbol{x}$. Based on this model, the next section introduces the proposed compression scheme.

A. *Compressed Sensing Model*

A Fourier subsampling compressed sensing strategy was studied for 3D SAFT in [10] where it was shown that subsampled Fourier matrices $\boldsymbol{F} \in \mathbb{C}^{N_F \times N_T}$ are adequate for sensing. As per one of the approaches in [10], N_F samples are taken centered at the transducer center frequency in order to build $\boldsymbol{F}$. For the spatial subsampling, we consider the selection matrices $\boldsymbol{S}_{M_T} \in \mathbb{R}^{M_T \times M}$ and $\boldsymbol{S}_{M_R} \in \mathbb{R}^{M_R \times M}$, which select M_T and M_R array elements, respectively, out of the total M. Moreover, we consider a *Kronecker model* where the same RX selection is used for each Tx element. With these considerations, a compressed, noiseless FMC measurement $\tilde{\boldsymbol{y}} \in \mathbb{C}^{N_F \cdot M_R \cdot M_T}$ is given by

$$\tilde{\boldsymbol{y}} = (\boldsymbol{S}_{M_T} \otimes \boldsymbol{S}_{M_R} \otimes \boldsymbol{F})(\boldsymbol{I}_M \otimes \boldsymbol{I}_M \otimes \boldsymbol{H})\boldsymbol{M}\boldsymbol{x}. \tag{5}$$

Let $\boldsymbol{\Phi} = (\boldsymbol{S}_{M_T} \otimes \boldsymbol{S}_{M_R} \otimes \boldsymbol{F}) \in \mathbb{C}^{N_F \cdot M_R \cdot M_T \times N_T \cdot M^2}$ and $\boldsymbol{A} = (\boldsymbol{I}_M \otimes \boldsymbol{I}_M \otimes \boldsymbol{H})\boldsymbol{M} \in \mathbb{C}^{N_T \cdot M^2 \times N_T \cdot N_x}$. With these definitions, a compressed measurement can be modeled as

$$\boldsymbol{y} = \boldsymbol{\Phi}\boldsymbol{A}\boldsymbol{x} + \boldsymbol{n} \in \mathbb{C}^{N_F \cdot M_R \cdot M_T} \tag{6}$$

with the noise vector $\boldsymbol{n}$ accounting for measurement noise and model inaccuracies.

B. *Inverse Problem*

The goal is now to reconstruct $\boldsymbol{x}$, i.e. $\boldsymbol{X}$, given the compressed measurements $\boldsymbol{y}$ based on (6). Since the number of defects is small, $\boldsymbol{X}$ and $\boldsymbol{x}$ can be considered sparse and we can reconstruct it by finding a solution to

$$\min_{\boldsymbol{x}} \|\boldsymbol{y} - \boldsymbol{\Phi}\boldsymbol{A}\boldsymbol{x}\|_2^2 + \lambda \|\boldsymbol{x}\|_1. \tag{7}$$

Problems of the form (7) can be solved with FISTA [11], which alternates between gradient descent for the data fidelity term $\|\cdot\|_2^2$ and thresholding for the proximal operator of $\|\cdot\|_1$. Following [5], the regularization parameter λ can be calculated as

$$\lambda = w_1 \|(\boldsymbol{\Phi}\boldsymbol{A})^{\mathrm{H}}\boldsymbol{y}\|_\infty \tag{8}$$

for some $0 \leqslant w_1 \leqslant 1$.

For the gradient descent step, an approximation to the largest singular value of $\boldsymbol{\Phi}\boldsymbol{A}$ must be found without storing

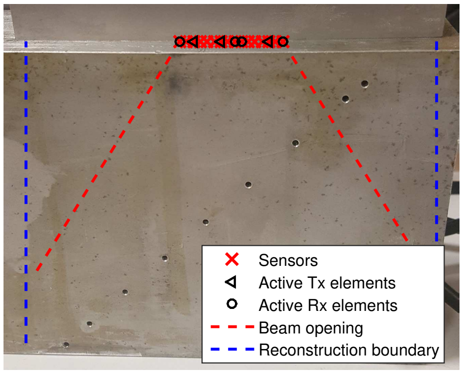

(a)

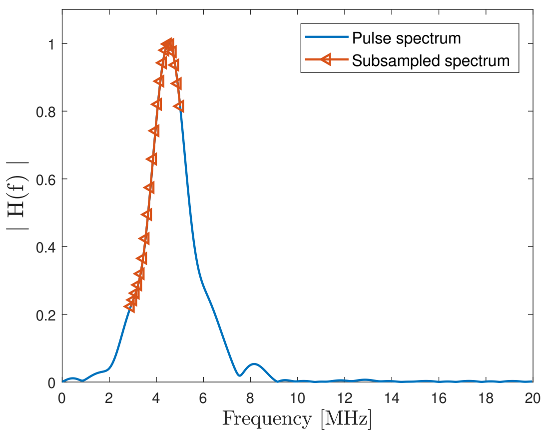

(b)

Fig. 2: Reconstructions scenario: (a) illustrates the active ULA elements for spatial subsampling and the reconstruction area overlaid on the test specimen, (b) shows the region of the pulse spectrum considered after Fourier subsampling.

the entire map [12], since it is impossible to do when the measurements and the reconstruction grid are large. The singular value is essentially the Lipschitz constant of the functional to be minimized in the gradient step. This constant's value must not be under-estimated, since then the function is assumed to be smoother than it actually is, which prevents FISTA from converging. Exploiting the structure of $\boldsymbol{A}$, the approximation is obtained as

$$\sigma_1 = w_2 \sqrt{\frac{M_R M_T N_T N_x}{2}} \|\boldsymbol{h}\|_2, \tag{9}$$

where $\boldsymbol{h} \in \mathbb{R}^{N_T \times 1}$ is a sampled pulse shape. Weight $w_2 \geq 1$ is included in case the algorithm does not converge, meaning the singular value has been underestimated. Suitable values have been experimentally determined to lie in the range $1 \leqslant w_2 \leqslant 10$. The impact of Fourier subsampling can be introduced by reducing $\|\boldsymbol{h}\|_2$ based on the bandwidth $N_F \cdot f_s / N_T$; this has been omitted, however, as it increases the risk of underestimating σ_1. As a final remark, FISTA entails an increased computational effort: for N_{FISTA} iterations, FISTA requires $2N_{\text{FISTA}}$ more matrix-vector products than TFM.

III. Reconstruction

To evaluate their performance, the proposed technique and standard TFM were tested on real measurement data. The specimen is a $12\,\text{cm}$ tall aluminium block with side drilled holes along its anti-diagonal and a speed of sound $c_0 = 6300\,\text{m}\,\text{s}^{-1}$. Data was gathered using the central $M = 16$ elements of a 64 element ULA at a sampling frequency of $f_s = 40\,\text{MHz}$, with $N_T = 1525$ samples per channel. The sensor pitch and opening angle are $\Delta_s = 1.8\,\text{mm}$ and $\theta = (8/45)\pi$, respectively. The reconstruction area spans the entirety of the array, with a grid of size $N_x = 321$, $N_T = 1525$ with $\Delta_x = 0.36\,\text{mm}$, $\Delta_z = 78.75\,\mu\text{m}$. A rough sketch of these parameters is shown in Fig. 2 to illustrate the scenario.

Compression is done synthetically by preserving $N_F = 81$ Fourier samples centered at $f_c = 4\,\text{MHz}$. Additionally, spatial subsampling is performed by selecting the channels corresponding to Rx elements $i = \{1, 9, 10, 16\}$ and Tx elements $j = \{3, 7, 14\}$ and discarding the rest. It should be noted that the selection matrices have an impact on the ability to detect arbitrarily placed reflectors and the presence of artifacts, and they should thus be obtained through optimization. Further details are left to future work. FISTA reconstructions are obtained after 100 iterations of the algorithm, using tuning parameters $w_1 = 0.05$, $w_2 = 2$, and $\sigma_1 = 4.0265 \times 10^4$.

Fig. 3a shows the result of performing standard TFM on the entire data set, with no subsampling. Three flaws are clearly visible along the anti-diagonal, and one more potential flaw on either side. Spatial subsampling reduces the number of measurement cycles from 16 to 3, considerably reducing the inspection time, and each cycle comprises 4 Rx elements. This comes at the cost of artifacts that reduce the resolution and make it difficult to determine the flaw locations correctly, as shown in Fig. 3b.

For comparison, the performance of FISTA applied to the entire data set is shown in Fig. 4a. The image appears more focused than Fig. 3a, with four flaws clearly visible and a potential fifth on the left side. Fourier and spatial subsampling are then applied, yielding the reconstruction in Fig. 4b. Although minor artifacts are present, four flaws are still visible. The achieved quality is vastly superior to that in Fig. 3b, performing close to TFM and FISTA with the entire data set. Most notably, the processed data volume contains only $0.25\,\%$ of the original number of samples, with $0.5\,\%$ of the size due to the usage of complex numbers.

IV. Conclusion

We have shown a compressed sensing model for FMC data that can reduce measurement times and data

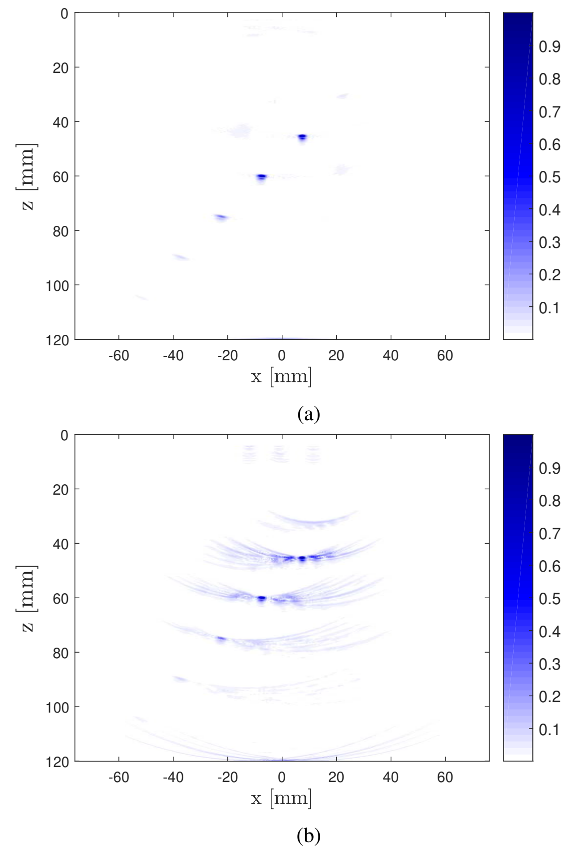

Fig. 3: Reconstructions using TFM. (a) was obtained using all the FMC measurement, while (b) exhibits artifacts due to spatial subsampling.

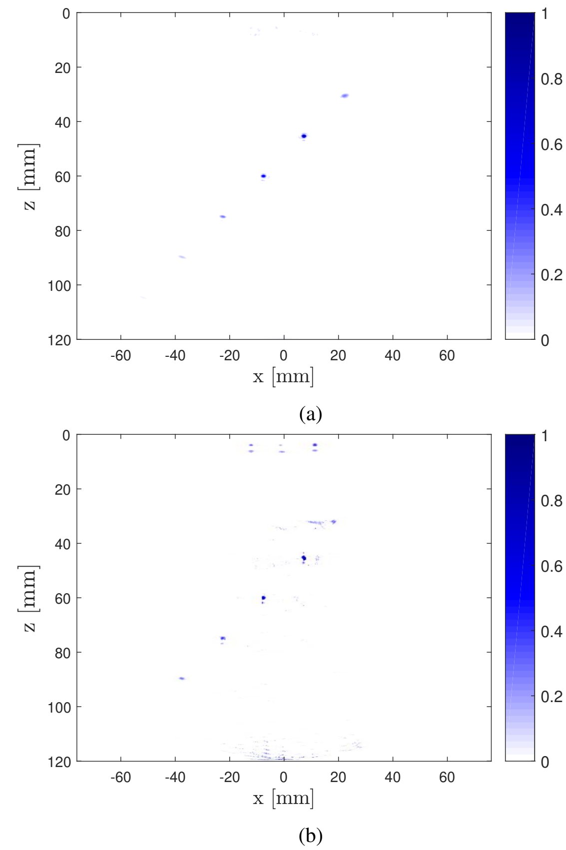

Fig. 4: Reconstructions using FISTA. The entire FMC data was used in (a). FISTA with Fourier and spatial subsampling results in (b), which is comparable to (a) in spite of using $0.25\,\%$ of the number of samples.

volumes through Fourier and spatial subsampling. Images reconstructed from such compressed measurements via FISTA exhibit good resolution, comparable to that of TFM and FISTA applied to complete data sets. The choice of channels and Fourier coefficients has an impact on the reconstruction quality and thus the design of the sensing matrix warrants further effort in future work.

References

[1] Andrey Bulavinov, Dieter Joneit, Michael Kröning, Ludwig von Bernus, Michael Dalichow, and Krishna Mohan Reddy. Sampling Phased Array A New Technique for Signal Processing and Ultrasonic Imaging. *ECNDT*, 2006.

[2] Alexander Velichko and Paul D. Wilcox. An analytical comparison of ultrasonic array imaging algorithms. *The Journal of the Acoustical Society of America*, 127(4):2377–2384, 2010.

[3] Caroline Holmes, Bruce W. Drinkwater, and Paul D. Wilcox. Post-processing of the full matrix of ultrasonic transmit–receive array data for non-destructive evaluation. *NDT & E International*, 38(8):701–711, 2005.

[4] Martin Spies, Hans Rieder, Alexander Dillhöfer, Volker Schmitz, and Wolfgang Müller. Synthetic Aperture Focusing and Time-of-Flight Diffraction Ultrasonic Imaging–Past and Present. *Journal of Nondestructive Evaluation*, 31(4):310–323, 2012.

[5] Ewen Carcreff, Nans Laroche, Dominique Braconnier, Aroune Duclos, and Sébastien Bourguignon. Improvement of the total focusing method using an inverse problem approach. In *2017 IEEE International Ultrasonics Symposium (IUS)*, pages 1–4. IEEE, 2017.

[6] Nicolas Quaegebeur and Patrice Masson. Correlation-based imaging technique using ultrasonic transmit–receive array for Non-Destructive Evaluation. *Ultrasonics*, 52(8):1056–1064, 2012.

[7] Nans Laroche, Ewen Carcreff, Sébastien Bourguignon, Jérôme Idier, and Aroune Duclos. An Inverse Approach for Ultrasonic Imaging by Total Focusing Point for Close Reflectors Separation. In *2018 IEEE International Ultrasonics Symposium (IUS)*, pages 1–4. IEEE, 2018.

[8] Hani Almansouri, Singanallur Venkatakrishnan, Charles Bouman, and Hector Santos-Villalobos. Model-based iterative reconstruction for one-sided ultrasonic nondestructive evaluation. *IEEE Transactions on Computational Imaging*, 5(1):150–164, 2019.

[9] David James. *On two random models in data analysis*. PhD thesis, G.-August-Universität Göttingen, 2017.

[10] S. Semper, J. Kirchhof, C. Wagner, F. Krieg, F. Römer, and G. Del Galdo. Defect detection from compressed 3-D ultrasonic frequency measurements. In *Proceedings of the 27th European Signal Processing Conference (EUSIPCO-2019)*, A Coruna, Spain, September 2019.

[11] Donghwan Kim and Jeffrey A. Fessler. Another look at the fast iterative shrinkage/thresholding algorithm (FISTA). *SIAM Journal on Optimization*, 28(1):223–250, 2018.

[12] Jan Kirchhof, Sebastian Semper, and Florian Römer. GPU-Accelerated Matrix-Free 3D Ultrasound Reconstruction for Nondestructive Testing. In *2018 IEEE International Ultrasonics Symposium (IUS)*, pages 1–4. IEEE, 2018.